Supplementary information for: Phase problem in the B-site Ordering of La_2CoMnO_6: Impact on Structure and Magnetism

R. Egoavil[2], S. Hühn[1], M. Jungbauer[1], N. Gauquelin[2], A. Béché[2], G. Van Tendeloo[2], J. Verbeeck[2], V. Moshnyaga[1]

[1]*Erstes Physikalisches Institut, Universität Göttingen, Friedrich-Hund-Platz 1, 37077 Göttingen, Germany*

[2]*EMAT, University of Antwerp, Groenenborgerlaan 171, 2020 Antwerp, Belgium*

Experimental details.

For TEM investigation, a ~25-50 nm thick LCMO/STO lamella was prepared perpendicular to the $[01\bar{1}]$ zone axis orientation of the $SrTiO_3$ substrate using focused ion beam milling. The atomically resolved EDX experiments were performed using an FEI X-Ant-EM microscope at the University of Antwerp, operated at 300 kV which offers a high efficiency EDX system with a collection solid angle close to 1 Sr [1]. Atomic resolution HAADF scanning transmission electron microscopy (STEM), EELS experiments were performed using the FEI Qu-Ant-EM microscope also at the University of Antwerp, operated at 300 kV. This is an FEI Titan3 microscope, equipped with aberration correctors for both image and probe forming lenses, and a monochromator to optimize the energy resolution for EELS measurements up to 0.1-0.2 eV, as determined from the full width at half maximum (FWHM) of the zero-loss peak (ZLP). The spatial resolution performance for HAADF imaging is ~0.8 Å (probe size) at a convergence semi-angle of 21.4 mrad. In order to extend the field of view spatially resolved 8192x8192 pixels^2 HAADF images were recorded with a detector collecting from 41.5 to 94.9 mrad. The electronic structure of Co-$L_{2;3}$, Mn-$L_{2;3}$ and O-K edges was investigated in monochromated STEM-EELS (Dual EELS mode) with a convergence semi-angle of 19 mrad providing an electron dose of 80 pA. An energy dispersion of 0.05 eV/pix was used to simultaneously record the low loss and core loss signals for each element for accurate determination of onset energies and fine structures. EELS elemental maps (see Figure SI1, supplementary information) were obtained with convergence and collection semi-angles of 21.4 and 94 mrad, respectively, with an acquisition time of 0.05 sec/pixel, a step size of 0.4 Å/pixel and energy dispersion of 0.25 eV/pixel, chosen to record simultaneously the corresponding signals for Co-$L_{2;3}$, Mn-$L_{2;3}$, La-$M_{4;5}$ and O-K edges in the sample.

Atomically resolved EELS maps of ordered and disordered regions.

EELS elemental maps for the Co-$L_{2;3}$, Mn-$L_{2;3}$, La-$M_{4;5}$, Ti-$L_{2;3}$ and O-K with atomic resolution are presented using gray scale code in Figure SI1. The EELS color map with Co (green), Mn (red) and La (blue) impeccably demonstrates the Co/Mn layered ordering obtained in the ordered phase (Ordered panel), while the Co/Mn ions are randomly distributed in the disordered phase (Disordered panel). These results are fully consistent with atomically resolved EDX maps presented in Figure 3 (main text).

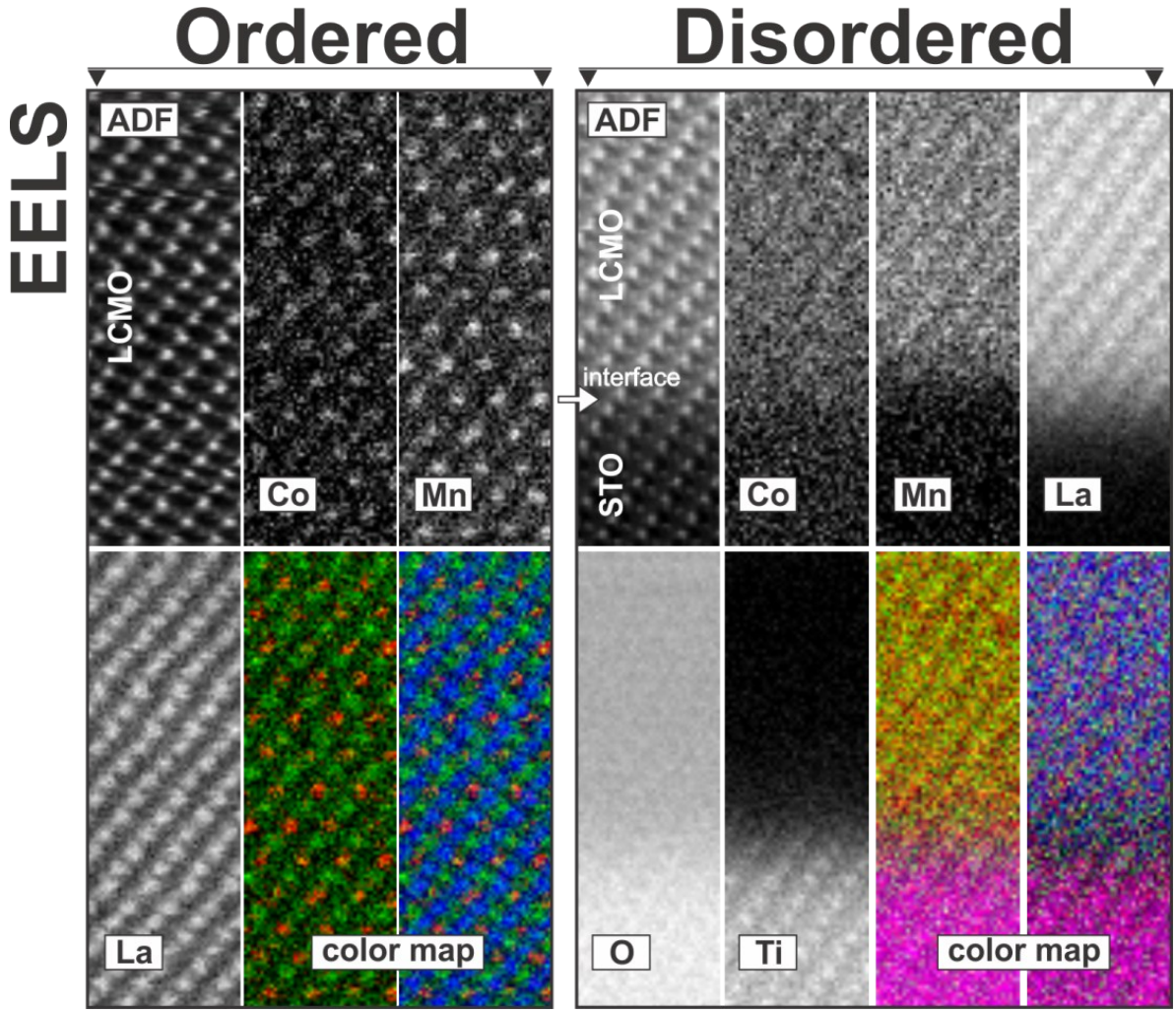

Figure SI1: Recorded atomic resolution ADF image and its corresponding EELS maps of a LCMO thin film. Chemical elemental maps of the ordered and disordered are shown in gray scale. The combined color map with Co (green), Mn (red), La (blue), Ti (magenta) demonstrates the Co/Mn cation arrangement in both phases.

Analysis of lattice distortions of ordered and disordered states.

In order to determine the lattice distortions in the La_2CoMnO_6 film, the HAADF intensity line profiles for the La and Co/Mn atomic positions corresponding to the two selected ordered and disordered regions are presented in Figure SI2. From these profiles we can observe small modulations in lattice parameter from a = 2.5 to 3.0 Å within the disordered region, while a nearly constant lattice parameter, a = 2.7 Å, is estimated in the ordered region.

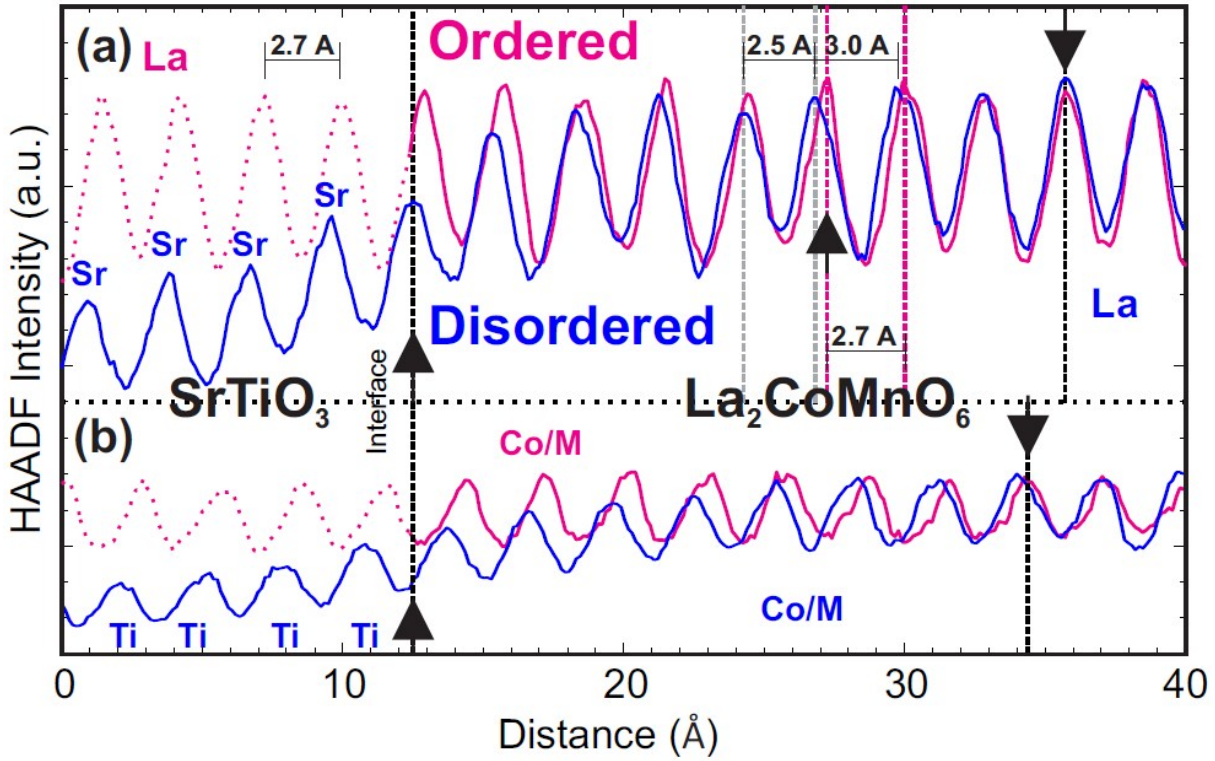

Figure SI2: HAADF intensity profiles for (a) La (La/Sr) and (b) Co/Mn (Ti) atomic positions in the ordered and disordered regions.

ELNES of the O-K edge.

The Oxygen K edges of oxides containing Mn and Co ions are reported by H. Tan et al. [2] to be strongly related to bond distances and coordination number. In spite of which, the fine structure of spectra of the oxygen K-edge acquired simultaneously for the ordered and disordered regions present only minor differences as shown in Figure 5. The O-K edge in this film consists of three main peaks (A, B, C) and a small peak C* in between B and C, different than the four peaks observed in the $SrTiO_3$ substrate. Two differences can be noticed: (1) the peak intensity in A (at ~529.3 eV) is slightly increased in the ordered phase, whereas (2) the spectral shape of B in the energy region of 533.9-535.9 eV deviates from one phase to another. The slight decrease of peak A can be related to a slight change of occupancy of the 3d levels of both cations, we can remark that this peak should be related to the disappearance of transitions to the t_{2g} states for Co^{2+} when going from high-spin (ordered phase) to low-spin (disordered phase). The observed changes of the peak in B, around 534 eV, are related to La-5d hybridized states and linked to the presence of two distinct La-O bond lengths in the ordered phase.

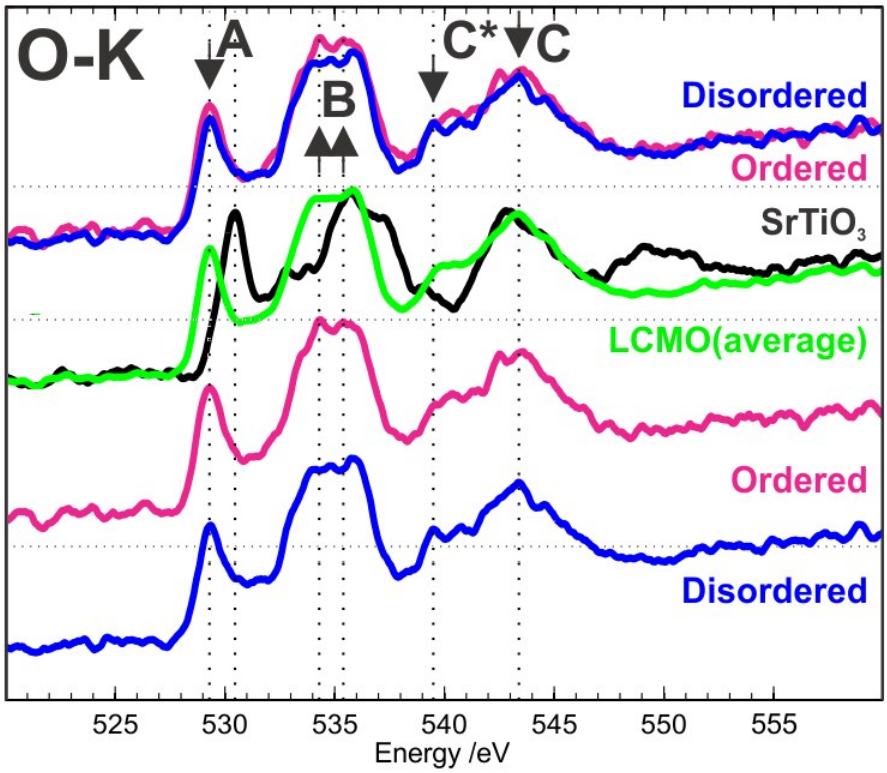

Figure SI3: O-K ELNES spectra in a La_2CoMnO_6 thin film. For clarity, all spectra are shifted vertically corresponding to both ordered (red) and disordered (blue) regions. The green curve is the integrated oxygen signal across the film and the curve in black is the oxygen signatures integrated the $SrTiO_3$ substrate region.

Multiplet calculations.

Multiplet calculations of Co and Mn 2p core-level spectra were performed using a version of Robert-Cowan's code (CTM4XAS), as implemented by F. DeGroot [3, 4]. All Co and Mn EELS spectra were compared to the simulated ones using the Co^{2+}, Co^{3+} and the Mn^{3+}, Mn^{4+} states, respectively. The charge transfer effects were included to simulate all ELNES spectra and their corresponding values of the parameters were taken from Bocquet et al. [5].

For cobalt ions, the Co^{2+}, Co^{3+} states were simulated in octahedral symmetry (Oh) [6] with the $3d^7$ and $3d^6$ electronic configurations, respectively. The initial and final states were described as mixtures of $3d^7 + 3d^8L$ and $2p^53d^8 + 2p^53d^9L$ configurations for Co^{2+}, and $3d^6 + 3d^7L$ and $2p^53d^7 + 2p^53d^8L$ for Co^{3+}, where L denotes a hole on the 2p ligand shell (valence band). To fit the experimental Co-$L_{2,3}$ spectral signatures, the crystal field strength of 10Dq = 0.90eV was used, while the 3d Slater integrals were set to 75% of their Hartree-Fock values. The charge transfer parameters were the following; the e_g = 2.0 eV and t_{2g} = 1.0 eV energy states, the charge transfer energy (Δ = 2.5 eV) and Coulomb interaction energy (U_{dd} = 4.2 eV, U_{pd} = -0.9 eV)[5]. On the other hand, a reduction of the crystal field strength 10Dq from 0.90 eV to 0.30 eV, as well as a jump to a higher e_g = 2.4 eV and t_{2g} = 1.2 eV energy levels were essential to reproduce the experimental spectra in the disordered phase.

For Mn ions, the Mn^{3+}, Mn^{4+} states were simulated in octahedral symmetry (Oh) [7] with the $3d^4$ and $3d^3$ electronic configurations, respectively. The initial and final states were described as mixtures of $3d^4 + 3d^5L$ and $2p^53d^5 + 2p^53d^6L$ configurations for Mn^{3+}, and $3d^3 + 3d^4L$ and $2p^53d^4 + 2p^53d^5L$ for Mn^{4+}. To fit the experimental Mn-$L_{2;3}$ spectral signatures, the crystal field strength of 10Dq = 2.2 eV was used, while the 3d Slater integrals were set to 30%, and an increment of 10% of the 2p spin-orbit coupling was necessary. The charge transfer parameters were the following; the e_g = 2.0 eV and t_{2g} = 1.0 eV energy states, the charge transfer energy (Δ = 2.0 eV) and Coulomb interaction energy (U_{dd} = 7.8 eV, U_{pd} = -1.5 eV)[5]. Here, in the disordered phase a substantial improvement to reproduce the experimental signatures is obtained by the introduction of tetragonal distortion (D4h) using crystal field strengths of 10Dq = 2.7 eV, Dt = 0.10 eV and Ds = 0.10 eV. Instrumental broadening was taken into account in all simulated spectra by using Gaussians and Lorentzians with FWHM of 0.25 - 0.3 eV.

X-ray reflectometry data and fit.

The X-ray reflectometry measurements were performed using the D8 Advance diffractometer by Bruker AXS. A copper anode was used as the X-ray source, the radiation of which was monochromatized with a Göbel mirror. The X-ray reflectometry simulation and fit were made with the ReMagX software [8]. The optical constants of LCMO were calculated with the data of the Chantler table [9].

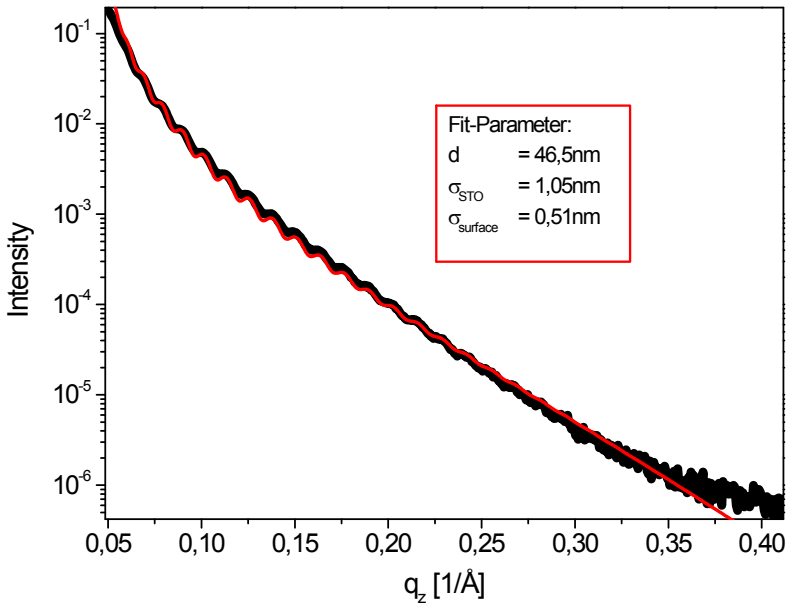

Figure SI4: Measured small angle X-ray reflectometry curve (black) of an LCMO/STO(111) film. The calculated thickness of the film is d = 46.5nm. The fit with ReMagX [8] (red) gives a surface mean-square roughness, RMS = 0.51nm, and the LCMO/STO interface roughness, RMS = 1.05nm.

XRD Simulation.

The structure factor F [10] of a perfectly ordered LCMO crystal model was calculated with the help of the atomic scattering factors f_n given by [11]:

$$F = \sum_{n=1}^{N} f_n \, exp\left(2\pi i\left(\vec{G} \cdot \vec{r}_n\right)\right)$$

with the position, $\vec{r}_n$, of the n^{th} atom in the unit cell with N atoms and the reciprocal lattice vector $\vec{G}$. The intensity I was calculated for a structure with M unit cells by:

$$I = \left| F \sum_{m=1}^{M} exp\left(i\left(\vec{G} \cdot \vec{R}_m\right)\right)\right|^2$$

with the position of the m^{th} unit cell $\vec{R}_m$. In the calculation of the XRD intensity the Cu-$K_{\alpha 1}$ and $K_{\alpha 2}$ radiation and the Lorentz polarization correction $(1 + \cos^2(2\theta))/(\sin^2(\theta)\cos(\theta))$, with the angle of the incident beam θ, was considered [10].

1. L. J. Allen, A. J. DAlfonso, B. Freitag, D. O. Klenov, Chemical mapping at atomic resolution using energy-dispersive x-ray spectroscopy, MRS BULLETIN 37 (2012) 47–52.

2. H. Tan, J. Verbeeck, A. Abakumov, G. Van Tendeloo, Oxidation state and chemical shift investigation in transition metal oxides by EELS, Ultramicroscopy 116 (2012) 24–33.

3. F. De Groot, A. Kotani, Core level spectroscopy of solids, CRC Press, Boca Raton FL, 2008.

4. This program can be downloaded from www.anorg.chem.uu.nl/CTM4XAS/.

5. A. E. Bocquet, T. Mizokawa, T. Saitoh, H. Namatame, A. Fujimori, Electronic structure of 3d-transition-metal compounds by analysisof the 2p core-level photoemission spectra, Phys. Rev. B 46 (1992) 3771–3784.

6. G. Radtke, S. Lazar, , G. A. Botton, High-resolution eels investigation of the electronic structure of ilmenites, Phys. Rev. B 74 (2006) 155117.

7. B. Gilbert, B. H. Frazer, A. Belz, P. G. Conrad, K. H. Nealson, D. Haskel, J. C. Lang, G. Srajer, , G. D. Stasio, Multiple scattering calculations of bonding and x-ray absorption spectroscopy of manganese oxides, J. Phys. Chem. 107 (2003) 2839–2847.

8. Macke, S., Brück, S., Audehm, P., Harlander, M. & Goering, E., ReMagX: X-ray Magnetic Reflectivity Tool, Available at www.mf.mpg.de/remagx.html (2009).

9. Cullity, B. D. & Stock, S. R., Elements of X-ray Diffraction, 3rd ed. (Prentice Hall, 2001).

10. Prince, E., in International Tables for Crystallography, Volume C: Mathematical, Physical and Chemical Tables (Springer, 2004), Vol. 3, p. 554.